

Expandable Li Percolation Network: The Effects of Site Distortion in Cation-Disordered Rock-Salt Cathode Material

Yujian Sun,[#] Sichen Jiao,[#] Junyang Wang, Yuanpeng Zhang,^{*} Jue Liu,^{*} Xuelong Wang,^{*} Le Kang, Qiqian Yu,^{*} Hong Li, Liqun Chen, and Xuejie Huang



Cite This: <https://doi.org/10.1021/jacs.3c02041>



Read Online

ACCESS |



Metrics & More

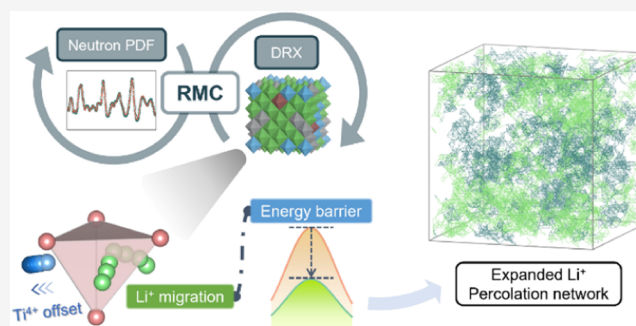


Article Recommendations



Supporting Information

ABSTRACT: Cation-disordered rock-salt (DRX) materials receive intensive attention as a new class of cathode candidates for high-capacity lithium-ion batteries (LIBs). Unlike traditional layered cathode materials, DRX materials have a three-dimensional (3D) percolation network for Li⁺ transportation. The disordered structure poses a grand challenge to a thorough understanding of the percolation network due to its multiscale complexity. In this work, we introduce the large supercell modeling for DRX material Li_{1.16}Ti_{0.37}Ni_{0.37}Nb_{0.10}O₂ (LTNNO) via the reverse Monte Carlo (RMC) method combined with neutron total scattering. Through a quantitative statistical analysis of the material's local atomic environment, we experimentally verified the existence of short-range ordering (SRO) and uncovered an element-dependent behavior of transition metal (TM) site distortion. A displacement from the original octahedral site for Ti⁴⁺ cations is pervasive throughout the DRX lattice. Density functional theory (DFT) calculations revealed that site distortions quantified by the centroid offsets could alter the migration barrier for Li⁺ diffusion through the tetrahedral channels, which can expand the previously proposed theoretical percolating network of Li. The estimated accessible Li content is highly consistent with the observed charging capacity. The newly developed characterization method here uncovers the expandable nature of the Li percolation network in DRX materials, which may provide valuable guidelines for the design of superior DRX materials.



1. INTRODUCTION

In the presence of climate change and the global energy crisis, the development of lithium-ion batteries (LIBs), the major chemical energy storage device, receives unprecedented attention during the transition from fossil fuels to sustainable energy resources. To fulfill the boosting energy needs from the electric vehicle market and smart grid construction, researchers focus on inventing novel high-energy-density LIB materials. Since Lee and Ceder's pioneering work¹ revealed that lithium ions can be accessed in the disordered rock-salt structure, lithium-excess disordered rock-salt (DRX) cathode material has become a rising star for the next generation of high-energy-density LIBs. The DRX material family has a general chemical formula of Li_{1+x}TM_{1-x}O₂ and shares a unified rock-salt (NaCl) structure where Li/TM cations distribute over one set of close-packed lattice of octahedral sites (Na sites) and O anions occupy the other (Cl sites). Different from conventional layer-structured cathode material (LiTMO₂) where Li ions can easily diffuse inside/out of the two-dimensional (2D) Li layer, the DRX material asks for a three-dimensional (3D) Li transportation network. Guided by theory, Lee and co-workers pointed out the key role of 0-TM Li diffusion channel, referring to the low-energy pathway bypassing a tetrahedral site

that shares face only with octahedral Li but no transition metal (TM) ions. Furthermore, they established the critical amount of excess Li ($x > 9\%$), namely, the Li percolation threshold, with which an infinite network can form throughout the 3D framework consisting of 0-TM diffusion channels. DRX materials break the constraints on element selection for designing conventional layer-structured cathode material and extend the exploration space to other low-cost and earth-abundant TMs besides Ni, Co, and Mn.

Many studies emerged on the optimization of DRX cathode materials to achieve high capacity and reversibility. In terms of compositional design, once exceeding the percolation threshold, further increment of Li content would in theory enlarge the Li percolation network, thus promoting the material's capacity.¹ Several experimental studies have reported charging capacity growth as the Li excess level increases from $x = 0$ to x

Received: March 1, 2023

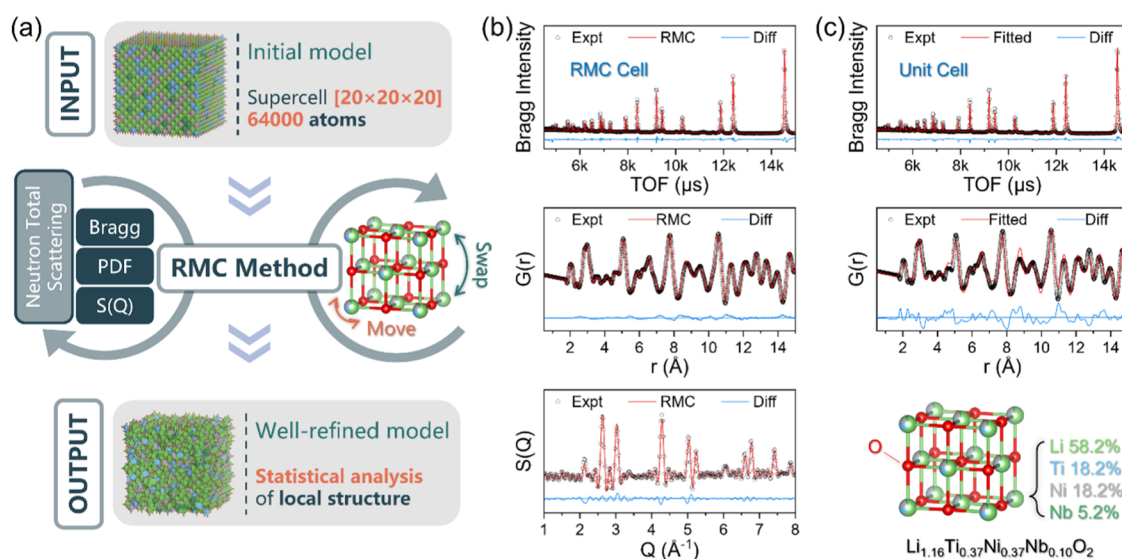


Figure 1. (a) Schematic for the workflow of RMC modeling and fitting. (b) RMC fitting results of Bragg, $G(r)$, and $S(Q)$ data. (c) Unit cell fitting results of Bragg and $G(r)$ data. The unit cell is shown in the inset, with the site occupancy and the stoichiometric formula annotated.

= 0.4.²⁻⁴ As Li content rises, the nominal valence state of TM cations rises to maintain charge neutrality and anion redox may be activated at a high state of charge (SOC). Mainstream optimization strategies are centering around these two challenges. On the cation side, the combination of multi-electron redox cations and high valence compensator cations has been constantly reported as a successful strategy. The multi-electron redox, such as Mn^{2+}/Mn^{4+} ,⁵⁻¹² Ni^{2+}/Ni^{4+} ,^{4,13-16} V^{3+}/V^{5+} ,¹⁷⁻²⁰ and Mo^{3+}/Mo^{6+} ,^{1,21,22} can provide the electron reservoir for deep Li deintercalation and help to increase the Li/TM ratio. The redox-inert TM cations of high valence act as charge compensators to fulfill the requirement of global charge balance. Soon it was discovered that some high-valence TM cations can help stabilize lattice oxygen at high SOC. For example, Yabuuchi et al.^{10,23} reported that high-valent Nb^{5+} in $Li_{1.3}Nb_{0.3}Mn_{0.4}O_2$ cathode stabilizes oxide ions at high voltage, leading to a high and reversible capacity of approximately 300 mAh g⁻¹ at 50 °C. Chen et al.²⁴ pointed out even better effects of Ti^{4+} in stabilizing oxide anions than Nb^{5+} . On the anion side, substituting oxygen anion with the less reducible fluorine anion has been reported as an effective way to achieve high energy densities up to 1000 Wh kg⁻¹. F^- can also elevate the ratio of low-valent multi-electron redox-active TM cations such as Ni^{2+} and Mn^{2+} .^{6,25} Besides compositional design, synthetic process optimization also draws attention. Well-controlled particle size would greatly benefit Li diffusion kinetics probably by shortening the Li migration path.^{3,10,26,27} Sintering temperature and duration could observably affect the structural disorder.^{28,29}

As studies dig deeper into DRX materials with different compositions, it was realized there is short-range cation order at the atomic scale. More specifically, cations are not randomly distributed over lattice sites as assumed. Local ordered cation arrangements, namely, short-range ordering (SRO), widely exist in DRX materials. The rules for SRO formation have not been fully elucidated. The ways of SRO pattern manifestation are various²⁹⁻³⁶ and closely related to the DRX material composition. Some high-valence d^0 cations, like Ti^{4+} , Nb^{5+} , and Mo^{6+} , were found critical in promoting cation mixing and breaking SRO.³⁷ Urban and co-workers established its

theoretical base that d^0 electronic configuration lowers the energy penalty for octahedral site distortion, which makes d^0 cations tolerant to site distortion caused by the mixing of cations in different sizes.³⁷ However, d^0 elements can lose their charm in certain element combinations. For example, Ji et al. compared the performance of $Li_{1.2}Mn_{0.4}Ti_{0.4}O_2$ and $Li_{1.2}Mn_{0.4}Zr_{0.4}O_2$.³⁰ Though both Ti^{4+} and Zr^{4+} are d^0 cation, Ti^{4+} renders a more random cation distribution than Zr^{4+} , resulting in better connectivity of 0-TM channels and higher capacity release. Evidently, the local structures of DRX materials strongly affect Li transportation and capacity performance. Yet, the relationship is very complicated, especially when covering multiple length scales. Site distortions may warp the tetrahedral channels through which Li ions diffuse. Each distorted cation site, together with its several neighbor sites, form small clusters, at which scale SRO manifest. In addition, multiple clusters stack together building up the crystalline framework Li percolation network embedded in. At the mesoscale, the size and connectivity of the Li percolation network directly decide the capacity and rate performance of the DRX material. The thermodynamically favored local segregation of specific TM cations may disrupt the Li^+ diffusion channel connection leading to a poor percolation network.^{32,38} Structures at the short to intermediate ranges all have non-negligible impacts on the overall capacity and kinetics of DRX material, urgently requiring in-depth investigation.

Albeit important, the multiscale characterization of the DRX local structure is challenging. Local structure characterization methods, including nuclear magnetic resonance spectroscopy (NMR), extended X-ray absorption fine structure spectroscopy (EXAFS), and Raman spectroscopy, reveal the bonding environment only in the nearest coordination shells.^{33,36,39} Electron microscopy techniques, such as high-resolution scanning transmission electron microscopy (HR-TEM), can identify partially ordered domains in a very small area of several hundreds of atoms.⁴⁰ The electron diffraction technique could validate the existence of SRO on a larger scale yet only in a semiquantitative manner.^{4,28} A method to quantitatively describe local structure variation throughout the

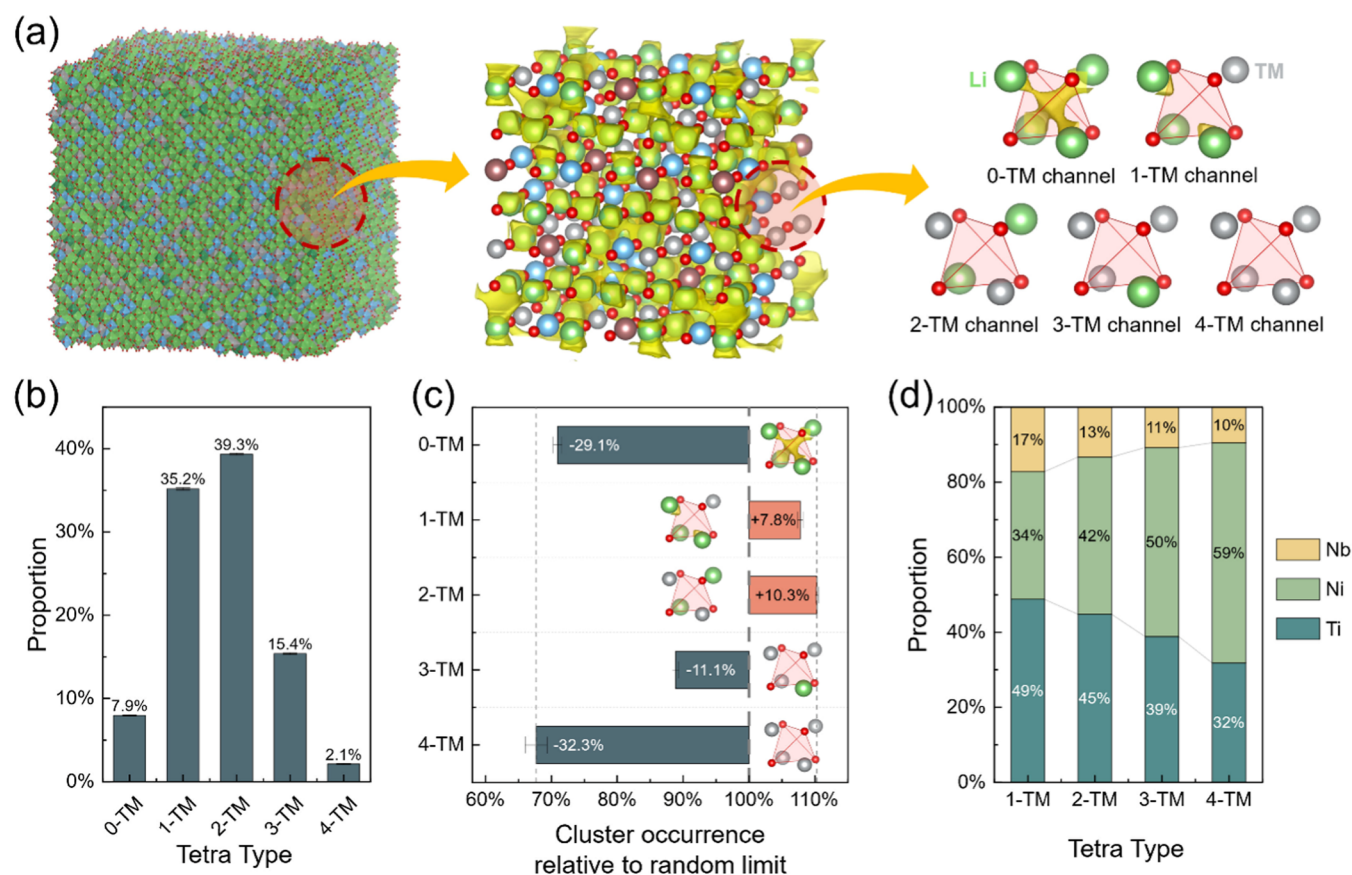


Figure 2. (a) Illustration of Li migration pathways in the modeled supercell. Green and red balls represent Li and O ions, and the other colored balls represent TM ions. The BV analysis result of Li⁺ migration pathways is shown as yellow iso-surfaces. (b) Cluster occurrence of different tetrahedral channel types. (c) Cluster occurrence of different tetrahedral channel types relative to the random limit. (d) TM composition of different types of tetrahedral channels.

global range is still needed. One means to hit this mark is the Monte Carlo (MC) supercell modeling combined with neutron pair distribution function (PDF) analysis, which contains abundant local structural information.^{30,35} However, limited by computational expense, it is still challenging for this method to achieve robust large-scale statistical reliability, considering the current supercell size (several hundreds of atoms at maximum). Different from MC methods based on energy minimization, the reverse Monte Carlo (RMC) modeling method, directly analyzing the experimental total scattering data,^{41,42} could describe local structure at both micro- and mesoscale. Through very large cell (tens of thousands of atoms) modeling, statistics on local structural details including the distribution of atomic position, bond lengths, and angles could be obtained.^{41,42} Early applications of the RMC method were mainly focused on liquid and amorphous materials like glass⁴³ and porous carbon.^{44–46} Subsequent developments enabled it to distinguish structural disorder in crystalline materials.⁴⁷ Additional explicit fitting of the Bragg intensities, extracted from the original total scattering data, ensures the atomic model to conform with the long-range lattice symmetry.⁴⁷ Studies using the RMC method on local ordering and distortion in crystal materials like high-entropy oxides⁴⁸ and electrode materials^{49,50} have been reported, inspiring us to apply it to the DRX system. In this work, a very large cell (20 × 20 × 20, containing 64 000 atoms) model was built, refined, and analyzed in detail for DRX cathode material Li_{1.16}Ti_{0.37}Ni_{0.37}Nb_{0.10}O₂ (LTNNO) via

the RMC method. We found that site distortions mostly related to Ti⁴⁺ are prevalent throughout the supercell. The site distortion could alter the Li⁺ migration barrier through tetrahedral channels, activating partial 1-TM channels for Li diffusion. The percolation network is successfully expanded containing accessible Li content in ideal consistency with the electrochemical measurement. Taking the unique advantage of the RMC method in statistically analyzing the complicated structure of DRX material, this work uncovered previously overlooked effects of local site distortion on expanding Li percolation network.

2. RESULTS AND DISCUSSION

2.1. RMC Modeling and Fitting Results. Figure 1a demonstrates the workflow we adopt using the RMC method in this work. First, to retain structural details across a length scale as wide as possible, a very large supercell model is built for Li excess DRX material Li_{1.16}Ti_{0.37}Ni_{0.37}Nb_{0.10}O₂. Then, three different forms of neutron total scattering data are included for fitting, namely, the Bragg diffraction data, the real space data $G(r)$, and the reciprocal space data $S(Q)$. Finally, all atoms in the supercell are iteratively swapped and moved until the best fit is reached. Each different form of data emphasizes a distinctive aspect of the structural feature, so the refined structural model is not biased. Typically, the real space PDF data focuses on the short-range correlation, whereas the reciprocal space Bragg diffraction data emphasizes the long-range correlation. For a data-driven approach like the RMC

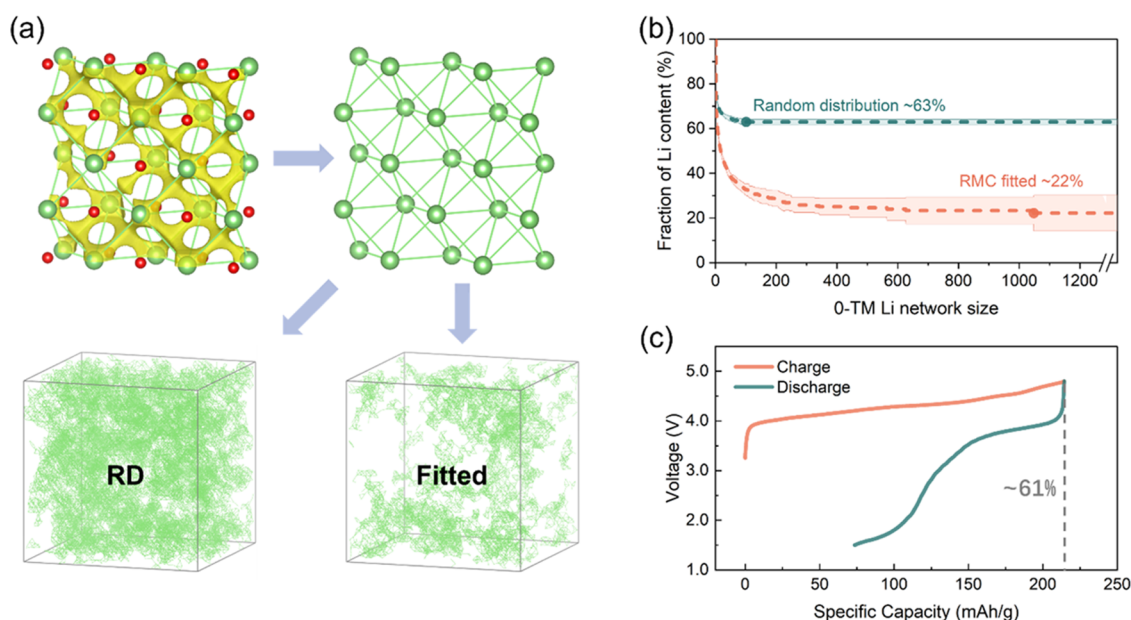


Figure 3. (a) Illustration of a Li^+ diffusion network extracted from a DRX supercell model. Instances of an RD supercell and an RMC-fitted supercell are plotted below. (b) Summarized Li contents in all Li^+ diffusion networks larger than a certain size. The final plateau of each curve denotes the fraction of Li contents in the maximum network. Both plots of the RD and RMC-fitted supercell are averaged over five independent runs, with the error bands denoting the standard errors. (c) First cycle voltage profile of LTNNO. The battery was charged to 4.8 V and discharged to 1.5 V at the current density of 10 mA g^{-1} with a swage-lock type cell configuration. The first-charge capacity of 214.4 mAh g^{-1} amounts to about 61% Li content, and the first-discharge capacity of 140.8 mAh g^{-1} amounts to 40.1% Li content.

method, the relevant structural features are magnified by the strong features (i.e., peaks) of corresponding data. The inclusion of Bragg data as a separate dataset beside $S(Q)$ minimizes the side effects of using a finite-size simulation box. Details about RMC fitting operation can be found in the [Supporting Information](#).

Figure 1b shows one of the final fitting results of the Bragg, $G(r)$, and $S(Q)$ data. More detailed fitting results could be referred to in [Figure S1](#). The black circles mark the original experimental data points, the red solid lines are calculated from the refined supercell model, and the blue solid lines show the difference between them. All three forms of scattering data are well fitted, indicating that the obtained supercell model restores the structural feature of DRX in both reciprocal and real space. Especially, the good fitting to PDF in the low- r region (below 5 Å) suggests a good restoration of very local structural features in the supercell model. For comparison, conventional unit cell refinements were also conducted. The short-range PDF patterns are poorly matched even though the long-range Bragg data is well fitted ([Figure 1c](#)). Via RMC modeling with a large supercell, not only the average lattice symmetry can be recovered, but also the short-to-medium range structural information could be fetched, which is lost for a great part in the conventional unit cell refinement. The well-refined large DRX supercell, with abundant local structural information, provides an ideal platform for the following statistical analysis of the DRX structural features.

2.2. Structural Feature Statistics and SRO Existence in LTNNO. In DRX materials, a short-range structure environment represented by cation clusters wrapping around tetrahedral Li site directly determines the connectivity of the Li^+ migration channel. [Figure 2a](#) demonstrates the multiscale picture of Li migration in the DRX lattice. The full-size DRX supercell model obtained through RMC fitting is shown on the left. In the middle, a zoomed-out local region of the large

supercell visualizes the detailed Li diffusion network by showing interconnected low-energy paths based on bond valence (BV) analysis. Different types of migration channels are exhibited on the right, classified by the number of octahedral TM ions in the cation cluster wrapping around the channel. Visualized by the space enclosed in the BV iso-surface, only the 0-TM tetrahedral site can provide a connected channel with an energy low enough for Li^+ migration. This is consistent with what Lee et al. previously proposed through computational simulation.¹

Detailed statistical analysis on the structural feature of the LTNNO sample was conducted through five independent RMC runs and results are summarized in [Figure 2b–d](#). The occurrence proportion of each tetrahedral channel type was counted in [Figure 2b](#) where the error bar denotes the standard deviation among five RMC runs. The narrow error bar indicates that the statistical results from RMC fitting are highly reproducible and reliable. In the LTNNO sample, 0-TM channels only account for $\sim 7.9\%$ of all tetrahedral channels, while 1-TM and 2-TM channels make up the majority accounting for 35.2% and 39.3%, respectively. Compared with a hypothetical random DRX lattice ([Figure 2c](#)), the occurrence of 0-TM channel is 29.1% less in LTNNO. In contrast, the occurrence of 1-TM and 2-TM channels surpass the random limit by 7.8% and 10.3%, respectively. Note that the theoretical random limits of cluster occurrence here are purely mathematical results from probability calculation based on the elemental composition, independent of any specific structure model. This result reminds us that the as-synthesized LTNNO material doesn't have a fully disordered structure but instead contains a certain form of SRO. Further analysis of the TM composition of each cation cluster type revealed the correlation between SRO and elements in LTNNO. As shown in [Figure 2d](#), the composition of TM elements shows a monotone change as the TM number in the cation cluster

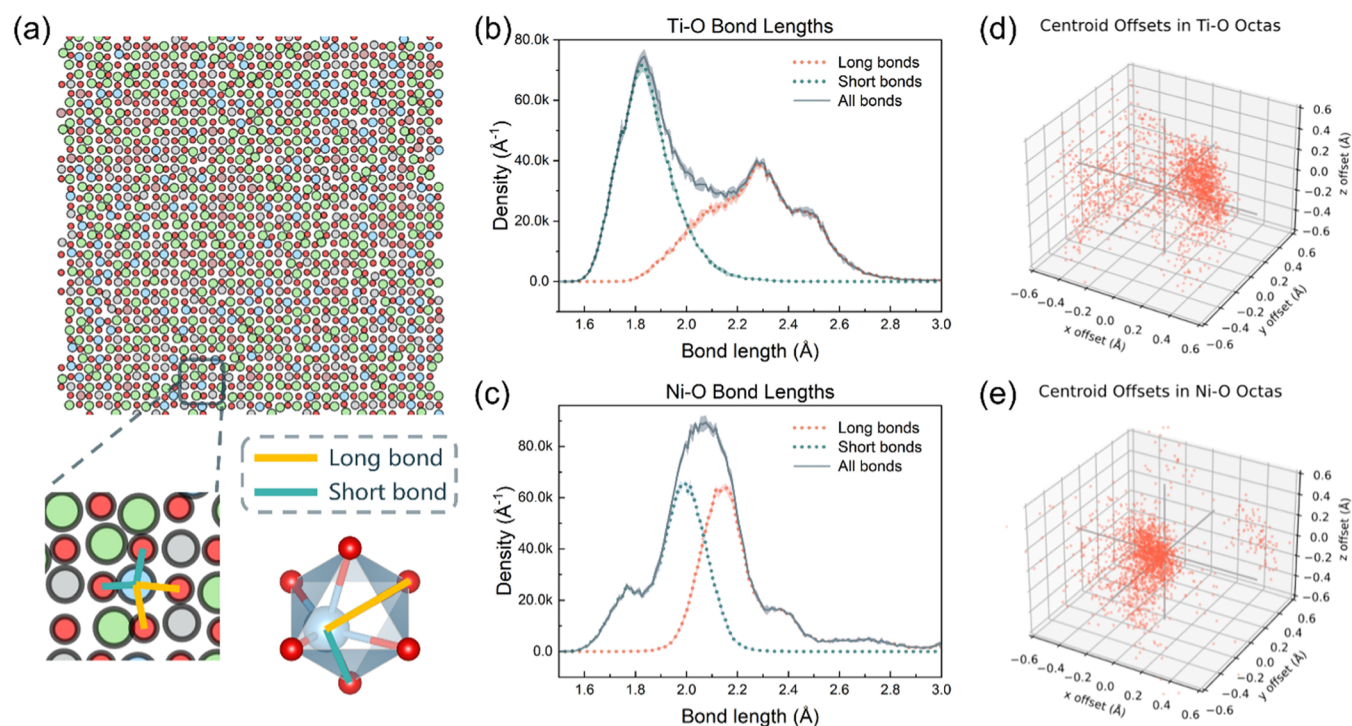


Figure 4. (a) 2D and 3D schematics of long and short bonds between Ti and O ions in a distorted lattice. (b) Ti–O and (c) Ni–O bond lengths distribution profile in the RMC-fitted supercell. The long bonds and short bonds are counted separately and plotted as orange and green dot lines. Scatter plots of centroid offsets in (d) Ti–O and (e) Ni–O octahedrons. Each red dot denotes the offset vector of one octahedron. The zero-offset references are indicated as the intersection of three axes plotted in gray solid lines.

increases. Specifically, the Ni^{2+} proportion continues to grow as TM cations populate and gets almost doubled in 4-TM clusters, while Ti^{4+} and Nb^{5+} make up the majority of 1-TM and 2-TM clusters but become the minority in 4-TM clusters. This phenomenon might be simply explained by the charge effects. High-valent TM cations like Ti^{4+} and Nb^{5+} tend to coordinate with low-valent Li^+ to maintain local charge balance, while the moderate valent Ni^{2+} could achieve charge neutrality with O^{2-} alone thus preferring secondary coordination with other Ni^{2+} cations. The element-dependent or chemistry-dependent SRO widely exists in DRX materials. For example, the current finding of Li–Ti and Ni–Ni clustering preference in LTNNO is in line with the previous theoretical investigations,⁵¹ where prominent Li–Ti and Ni–Ni clusterings were found in a DRX material $\text{Li}_{1.0}\text{Ti}_{0.5}\text{Ni}_{0.5}\text{O}_2$. Regarding the Nb^{5+} cations, Semykina et al. pointed out that, in a $\text{Li}_{1.3}\text{Nb}_{0.3}\text{Mn}_{0.4}\text{O}_2$ system, the presence of Nb^{5+} tends to prompt the segregation of Mn^{3+} cations.⁵²

In the view of thermodynamics, the formation of SRO in DRX material is driven by the preferred phase segregation at the low temperature, thus resembling the structural features of its ground state. The existence of such structurally ordered domains strongly affects Li^+ mobility within DRX material. For example, Wang et al. systematically studied the SRO in a series of Mn- and Fe-based DRX materials and revealed the widespread existence of layered-like domains.³⁶ The shuffled layer scheme they proposed for the DRX structure model may be beneficial for percolating Li diffusion. In current LTNNO material, the Ni-rich 4-TM clusters and Ti-rich 1-TM clusters are reminiscent of the NiO and Li_2TiO_3 structure, respectively, implying the formation of NiO- and Li_2TiO_3 -like domains. Therefore, the lithium percolating behavior under the influence of SRO requires further in-depth investigation for LTNNO.

2.3. Estimation of Percolating Li Content Based Solely on 0-TM Activation. Following the same procedure Ceder et al. previously took in analyzing the Li^+ percolation network of DRX materials with SRO,³⁰ Li sites connected by activated 0-TM tetrahedral channels were taken into a single diffusion network attributed as one Li cluster (Figure 3a). Comparison between the situation in random distribution (RD) and the RMC-fitted supercells clearly demonstrates the strong impact of SRO on the 0-TM-based Li^+ diffusion network. As visualized, the RD structure has a large and uniform percolation network filling the entire supercell while the fitted structure has a much sparser percolating network with large blank spaces out of reach.

A quantitative summarization of Li^+ percolation based solely on the 0-TM activating criterion is shown in Figure 3b. According to the percolation theory, the maximum Li cluster includes all accessible Li^+ once Li^+ percolation is formed and Figure 3b depicts the change of 0-TM-percolated Li content in the diffusion network as the size of the maximum Li cluster grows. Detailed network size profiles of the five RMC-fitted supercell models are presented in Figure S2. Both the curves of RD and RMC-fitted structures drop rapidly at the very beginning, indicating that a large portion of Li^+ is isolated in small clusters (below 100 Li ions). As the cluster size grows, the curves reach a plateau denoting the fraction of maximum 0-TM-percolated Li content. The calculated value in the fitted structures turns out 22% on average, much smaller than the value of 63% in the RD structures which could be attributed to the influence of SRO. The result is compared with the electrochemically accessible Li content presented by first cycle voltage profile of LTNNO in Figure 3c. The as-synthesized DRX material was charged to 4.8 V in the first cycle at the current density of 10 mA g^{-1} , exhibiting a first-charge capacity

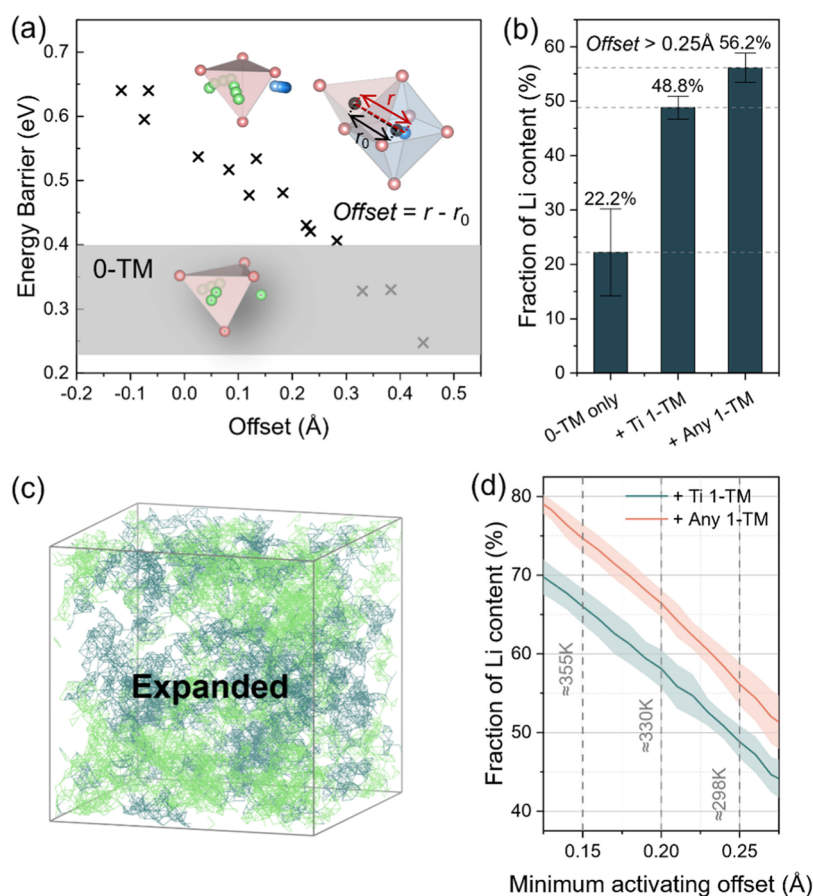


Figure 5. (a) DFT-calculated Li^+ migration energy barriers of Ti 1-TM channels relative to Ti offset values. Each cross denotes the energy barrier value calculated from one tetrahedral channel. The gray band denotes the energy barrier range of the 0-TM channels. (b) Fraction of Li content in the maximum Li^+ diffusion network after the activation of 1-TM channels with a TM offset value larger than 0.25 Å. The result under 0-TM-only activation is also given as a reference. (c) Expanded Li^+ diffusion network after 1-TM activation. The original 0-TM diffusion network is plotted in light green, and the expanded part of the network is plotted in dark blue. (d) Fraction of Li contents in the maximum Li^+ diffusion network relative to minimum TM offset for activating a 1-TM channel. The equivalent temperatures for reaching such minimum activating offsets are annotated beside the vertical dashed reference lines.

of 214.4 mAh g^{-1} which amounts to about 61% of the total Li content extracted from the material. (The same results can be obtained in the coin cell testing, as shown in Figure S3) Upon following discharge to 1.5 V, 140.8 mAh g^{-1} reversible capacity was obtained, referring to 40.1% Li content re-intercalated into the DRX lattice. Neither the first charge nor discharge capacity matches the accessible Li content proposed based solely on 0-TM percolation.

We notice that similar discrepancies have also been discovered in some previous works. For example, Ji et al.³⁰ compared two similar DRX materials $\text{Li}_{1.2}\text{Mn}_{0.4}\text{Zr}_{0.4}\text{O}_2$ (LMZO) and $\text{Li}_{1.2}\text{Mn}_{0.4}\text{Ti}_{0.4}\text{O}_2$ (LMTO). The SRO in LMTO facilitates the formation of more 0-TM channels and therefore a larger percolating network than that in LMZO, which qualitatively explains why LMTO exhibits superior electrochemical performance to LMZO. However, the ~35% percolating Li content in LMTO calculated under the assumption of sole 0-TM percolation does not match the high charge capacity (~1.0 Li per formula) obtained in electrochemical experiments.³⁰ These results imply that the sole 0-TM diffusion hypothesis may overlook some other diffusion mechanisms originating from DRX's unique structural features related to SRO.

2.4. Site Distortions Related to Cation Species. For most DRX materials, more than one species of TM cations coexist in the same set of cubic lattice sites. Local site size distortions have been reported before due to the large cation size differences which could be one origin of SRO formation.^{30,37} The locally ordered domain described by SRO may also aggravate the site distortion due to lattice strain imposed by different domain stacking. Obvious site distortions indeed prevail in current LTNNO material. Figure 4a visualizes the 2d projection of a typical plane of ion positions sliced from the RMC-fitted supercell structure. It can be intuitively seen that the oxygen ions generally stay close to the cubic lattice sites forming a fairly regular anion lattice frame. However, a large portion of cations is displaced from the octahedral center position. As shown in the magnified area of the plane, one Ti^{4+} ion (blue dot) is displaced toward the upper left. For a typical distorted TiO_6 octahedral, such site distortion means Ti^{4+} being closer to one of the eight octahedral faces than the others, which shortens its distance to three lattice oxygen ions while getting away from the other three. Consequently, the Ti–O bond lengths diverge, marked by orange and green solid lines, respectively. A universal profile of Ti–O bond length distribution is shown in Figure 4b, where it splits into two subpeaks centered around 1.8 and 2.3 Å. In

contrast, the Ni–O bond length profile appears to be a single peak centered around 2.1 Å (Figure 4c). Although two underlying short/long bond subpeaks still exist, they lay close to each other at around 2.0 and 2.2 Å, indicating nearly no site distortion arises from NiO₆ octahedral.

The statistics of centroid offsets, defined as the displacement from the center of a TMO₆ octahedron to the actual position of the cation, provide another perspective to view the TM site distortion. The distribution of cation offsets is collected throughout the supercell and plotted in a 3D cartesian coordinate space (Figure 4d,e). For Ti⁴⁺ in TiO₆ octahedra, most offset vectors fall at a certain distance from the origin, proving that the Ti⁴⁺ displacements are pervasive in LTNNO material. In contrast, an almost zero-centered distribution of offset vectors is observed for Ni²⁺ in the NiO₆ cathedral. These results accord well with Urban et al.'s theoretical work.³⁷ From the perspective of the electronic structure, cations with d⁰ electronic configuration like Ti⁴⁺ are insensitive to any type of site distortion within a TMO₆ octahedral, owing to the absence of electrons in the TM-dominated bands. However, TM cations filled by more than one d electron such as Ni²⁺ (d⁸) endure considerable energy penalty with the site distortion, which could destabilize the entire structure. The addition of d⁰ TM cations, such as Ti⁴⁺ can balance out unwanted site distortions within the DRX material, allowing other TM ions, such as Ni²⁺ to reside in an almost ideal geometry. Distortions of octahedrally coordinated d⁰ TM cations have been well-recognized and correlated with plentiful properties of materials,⁵³ like piezoelectricity, ferroelectricity, and nonlinear optical behavior, which can be ascribed to the second-order Jahn–Teller effect. We also examined the Nb–O bond length profile (Figure S4) since Nb⁵⁺ is also a d⁰ metal like Ti⁴⁺. Interestingly, the peak splitting of Nb–O bond lengths is not as apparent as Ti–O bond lengths. Although the statistical significance of the result may not be as robust as those of the other two transition metal species because the number of Nb⁵⁺ sites is relatively small, it is very likely that this is related to the second-coordination environments, which calls for further investigation.

The effects of TiO₆ distortion could be more than balancing out other TM's site distortion. Since Li–Ti prefers clustering in LTNNO as revealed by SRO analysis, the widespread TiO₆ distortion may affect the migration behavior of its neighboring Li⁺. The migration energy barrier (E_m) of lithium ions in solids is governed by the transitional site's local environment which is the atomic environment of the tetrahedral site in the scenario of DRX, including its geometry and the neighboring element species. In terms of geometric factors, Lee and co-workers revealed that the E_m of 1-TM channels is inversely proportional to tetrahedral height.¹ In layered cathodes like LiCoO₂, 1-TM channel activation is enabled by tetrahedral height being big enough. However, in the DRX structure tetrahedral height is usually too small to activate the 1-TM channel. In terms of the surrounding TM species, it can determine the electrostatic repulsion Li⁺ feels at the tetrahedral site. For example, 1-TM channels involving low-valence TM species are expected to have smaller E_m . Theoretically, if the TM cation drifts away from the transitional tetrahedral site, the migration barrier could be lowered. Site distortions may have a positive effect on lithium transport. The impacts of TM site distortions on the E_m and Li⁺ percolation network need to be investigated.

2.5. Impact of Cation Offsets on Li⁺ Diffusion. Based on the divacancy migration mechanism, in the DRX structure,

1-TM channels are the only type of tetrahedral channels that has the potential to be activated beside the 0-TM channels. To evaluate the effect of site distortions on Li⁺ mobility, we adopted MC modeling and DFT calculation to evaluate the E_m changing of 1-TM channels when the surrounding TM cation drifts from the original octahedral center. The details are described in the Supporting Information (Figures S5–S8). The distance between a tetrahedral center to its adjacent octahedral center is denoted as the original distance r_0 , as illustrated in the inset of Figure 5a. At a distorted site, the actual distance of the TM ion to the center of the tetrahedron is denoted as changed distance r . The cation offset is defined as the difference between r and r_0 , which can be positive or negative depending on whether the TM ion moves away or toward the tetrahedron.

Since most TM offsets observed are attributed to Ti⁴⁺, Ti 1-TM channels are selected for the calculation of E_m changing (Figure 5a). As the offset value increases, the Ti⁴⁺ ion drifts away from the tetrahedron, and the calculated E_m value drops in a monotonic trend. When the offset value reaches around 0.25 Å, the E_m drops below 0.4 eV, which falls into the range of 0-TM migration energies. Therefore, once the cation offset of a Ti 1-TM channel reaches above 0.25 Å, it can be considered activated for Li⁺ migration. Under this updated criterion, we calculated the elevated accessible Li fraction based on the percolating theory. The results are shown in Figure 5b. When counting in Li sites involved in Ti⁴⁺ 1-TM channel with offsets larger than 0.25 Å, the percolating Li content is promoted to 48.8% on average. If we also include the activation of Ni/Nb 1-TM channels using the same criterion (cation offset > 0.25 Å), the percolating Li content could be further promoted to 56.2%, very close to 61%, the measured fraction of Li content extracted from the material in the first cycle charging process. Furthermore, we also take the geometry factor into account, which can significantly vary the migration barrier, as the previous study indicated.¹ In the case of diffusion along the 1-TM channel, a smaller tetrahedral volume poses a higher migration barrier. Therefore, we extract the statistical distribution of tetrahedral site volume involved in the 1-TM diffusion channel within the supercell that was derived from the RMC fitting. As shown in Figure S9, the average tetrahedral site volumes around the NiO₆ and TiO₆ are around 3.18 and 3.02 Å³, respectively. To some extent, the smaller tetrahedral site volumes for the Ti 1-TM diffusion channel rule out the potential influence of geometry factors, corroborating that the reduced migration barrier is caused solely by the site distortions. These results successfully fill the large gap lying between the measured capacity and the theoretically calculated accessible Li content considering only 0-TM percolation (Figure 5c).

The potential of 1-TM channel activation on promoting the DRX performance inspires us to treat the problem from another angle. Looking at the Arrhenius relationship $D \sim e^{-E_m/k_B T}$, where D is the diffusion coefficient, T denotes the environmental temperature, and E_m and k_B are invariant to T . We can imagine that increase in temperature would increase the diffusion coefficient related to the channels, thus activating more 1-TM channels with a smaller offset for Li diffusion. If the environmental temperature is elevated to around 330 K from 300 K, the activating offset could be lowered to 0.20 Å. In this case, the percolating Li content could be lifted to 58% considering Ti 1-TM activation and 66% considering Ni/Nb 1-TM activation in addition (Figure 5d). If the temperature is

further elevated to around 355 K, the theoretically accessible Li content could reach 75% (above 260 mAh g⁻¹) considering the activation of any 1-TM channels with cation offsets surpassing 0.15 Å. This mechanism of 1-TM channel activation may contribute, at least partly, to the previously reported capacity boost of DRX cathodes under elevated temperatures.^{23,54,55}

Although additional factors including stability issues, capacity retention, and usage scenario should be further considered, the results suggest the possibility of achieving high-capacity DRX with offsets of specific cation species via elevated temperature.

3. CONCLUSIONS

Through large supercell modeling and RMC fitting to the neutron total scattering data, we obtained DRX models retaining the original material's structural feature across a short-to-long range. Good quality of fitting to Bragg, $G(r)$, and $S(Q)$ experimental data validate the adequacy of the RMC-refined supercell. Statistical local structural analysis shows that the preference of high-valent Ti⁴⁺ and Nb⁵⁺ to coordinate with Li⁺ ions results in a reduced number of 0-TM channels compared to the random limit. The calculated accessible Li content based on the 0-TM diffusion hypothesis is significantly smaller than the measured charge capacity. An in-depth investigation of the refined supercell's local structures reveals that the pervasive cation offsets, mostly related to Ti⁴⁺ ions, are responsible for partial 1-TM channel activation. Via DFT calculation, we offered the offset criterion for activating 1-TM channels. An expanded percolating network of accessible Li is constructed, conforming well with the measured capacity from electrochemical experiments. Further calculations suggest increasing temperature could lift accessible Li contents by expanding the percolation network to more 1-TM channels. Thanks to the unique capability of large supercell RMC modeling in combination with neutron total scattering, statistical structure information covering multiple scales is obtained. Results justified the previously reported site distortions in the DRX material and directly linked it to the capacity performance. The descending migration barrier against the increasing TM site offset guided us to bring up the mechanism of 1-TM channel activation, supplementary to the widely accepted 0-TM Li⁺ diffusion scheme. The large supercell modeling and RMC fitting method could be utilized as a powerful tool in the future to study complex DRX material covering multiple length scales, especially at the local range where site distortions and SRO manifest.

■ ASSOCIATED CONTENT

SI Supporting Information

The Supporting Information is available free of charge at <https://pubs.acs.org/doi/10.1021/jacs.3c02041>.

Additional details about the experimental procedure, RMC modeling details, statistical analysis method, and DFT calculation details (PDF)

■ AUTHOR INFORMATION

Corresponding Authors

Yuanpeng Zhang – Neutron Scattering Division, Oak Ridge National Laboratory, Oak Ridge, Tennessee 37831, United States; orcid.org/0000-0003-4224-3361; Email: zhangy3@ornl.gov

Jue Liu – Neutron Scattering Division, Oak Ridge National Laboratory, Oak Ridge, Tennessee 37831, United States; orcid.org/0000-0002-4453-910X; Email: liuj1@ornl.gov
Xuelong Wang – Beijing Frontier Research Center on Clean Energy, Institute of Physics, Chinese Academy of Sciences, Beijing 100190, China; Email: wangxuelong@iphy.ac.cn
Xiqian Yu – Beijing Frontier Research Center on Clean Energy, Institute of Physics, Chinese Academy of Sciences, Beijing 100190, China; Center of Materials Science and Optoelectronics Engineering, University of Chinese Academy of Sciences, Beijing 100049, China; orcid.org/0000-0001-8513-518X; Email: xyu@iphy.ac.cn

Authors

Yujian Sun – Beijing Frontier Research Center on Clean Energy, Institute of Physics, Chinese Academy of Sciences, Beijing 100190, China; Center of Materials Science and Optoelectronics Engineering, University of Chinese Academy of Sciences, Beijing 100049, China
Sichen Jiao – Beijing Frontier Research Center on Clean Energy, Institute of Physics, Chinese Academy of Sciences, Beijing 100190, China; Center of Materials Science and Optoelectronics Engineering, University of Chinese Academy of Sciences, Beijing 100049, China
Junyang Wang – Beijing Frontier Research Center on Clean Energy, Institute of Physics, Chinese Academy of Sciences, Beijing 100190, China; Center of Materials Science and Optoelectronics Engineering, University of Chinese Academy of Sciences, Beijing 100049, China; orcid.org/0000-0001-6025-5986
Le Kang – Institute of High Energy Physics, Chinese Academy of Sciences, Beijing 100049, China; Spallation Neutron Source Science Centre, Dongguan 523803, China
Hong Li – Beijing Frontier Research Center on Clean Energy, Institute of Physics, Chinese Academy of Sciences, Beijing 100190, China; Center of Materials Science and Optoelectronics Engineering, University of Chinese Academy of Sciences, Beijing 100049, China; orcid.org/0000-0002-8659-086X
Liquan Chen – Beijing Frontier Research Center on Clean Energy, Institute of Physics, Chinese Academy of Sciences, Beijing 100190, China
Xuejie Huang – Beijing Frontier Research Center on Clean Energy, Institute of Physics, Chinese Academy of Sciences, Beijing 100190, China; orcid.org/0000-0001-5900-678X

Complete contact information is available at: <https://pubs.acs.org/doi/10.1021/jacs.3c02041>

Author Contributions

*Y.S. and S.J. contributed equally to this work.

Notes

The authors declare no competing financial interest.

■ ACKNOWLEDGMENTS

This work was supported by funding from the National Natural Science Foundation of China (Grant No. U1932220) and CAS Project for Young Scientists in Basic Research (Grant No. YSBR-058). This work was partially supported by UT-Battelle, LLC, under Contract No. DE-AC05-00OR22725 with the US Department of Energy. The United States Government retains, and the publisher, by accepting the article for

publication, acknowledges that the United States Government retains a nonexclusive, paid-up, irrevocable, worldwide license to publish or reproduce the published form of this manuscript, or allow others to do so, for United States Government purposes. The DOE will provide public access to these results of federally sponsored research in accordance with the DOE Public Access Plan (<http://energy.gov/downloads/doepublic-accessplan>).

REFERENCES

- (1) Lee, J.; Urban, A.; Li, X.; Su, D.; Hautier, G.; Ceder, G. Unlocking the potential of cation-disordered oxides for rechargeable lithium batteries. *Science* **2014**, *343*, 519–522.
- (2) Chen, D.; Kan, W. H.; Chen, G. Understanding performance degradation in cation-disordered rock-salt oxide cathodes. *Adv. Energy Mater.* **2019**, *9*, No. 1901255.
- (3) Kobayashi, Y.; Sawamura, M.; Kondo, S.; Harada, M.; Noda, Y.; Nakayama, M.; Kobayakawa, S.; Zhao, W.; Nakao, A.; Yasui, A.; Rajendra, H. B.; Yamanaka, K.; Ohta, T.; Yabuuchi, N. Activation and stabilization mechanisms of anionic redox for Li storage applications: Joint experimental and theoretical study on Li_2TiO_3 – LiMnO_2 binary system. *Mater. Today* **2020**, *37*, 43–55.
- (4) Lun, Z.; Ouyang, B.; Cai, Z.; Clément, R. J.; Kwon, D.-H.; Huang, J.; Papp, J. K.; Balasubramanian, M.; Tian, Y.; McCloskey, B. D.; Ji, H.; Kim, H.; Kitchaev, D. A.; Ceder, G. Design principles for high-capacity Mn-based cation-disordered rocksalt cathodes. *Chem* **2020**, *6*, 153–168.
- (5) Freire, M.; Kosova, N. V.; Jordy, C.; Chateigner, D.; Lebedev, O. I.; Maignan, A.; Pralong, V. A new active Li-Mn-O compound for high energy density Li-ion batteries. *Nat. Mater.* **2016**, *15*, 173–177.
- (6) Lee, J.; Kitchaev, D. A.; Kwon, D. H.; Lee, C. W.; Papp, J. K.; Liu, Y. S.; Lun, Z.; Clement, R. J.; Shi, T.; McCloskey, B. D.; Guo, J.; Balasubramanian, M.; Ceder, G. Reversible $\text{Mn}^{2+}/\text{Mn}^{4+}$ double redox in lithium-excess cathode materials. *Nature* **2018**, *556*, 185–190.
- (7) Freire, M.; Lebedev, O. I.; Maignan, A.; Jordy, C.; Pralong, V. Nanostructured Li_2MnO_3 : a disordered rock salt type structure for high energy density Li ion batteries. *J. Mater. Chem. A* **2017**, *5*, 21898–21902.
- (8) Freire, M.; Diaz-Lopez, M.; Bordet, P.; Colin, C. V.; Lebedev, O. I.; Kosova, N. V.; Jordy, C.; Chateigner, D.; Chuvilin, A. L.; Maignan, A.; Pralong, V. Investigation of the exceptional charge performance of the $0.93\text{Li}_{4-x}\text{Mn}_2\text{O}_5 \cdot 0.07\text{Li}_2\text{O}$ composite cathode for Li-ion batteries. *J. Mater. Chem. A* **2018**, *6*, 5156–5165.
- (9) Kataoka, R.; Taguchi, N.; Kojima, T.; Takeichi, N.; Kiyobayashi, T. Improving the oxygen redox stability of NaCl-type cation disordered Li_2MnO_3 in a composite structure of Li_2MnO_3 and spinel-type LiMn_2O_4 . *J. Mater. Chem. A* **2019**, *7*, 5381–5390.
- (10) Yabuuchi, N.; Takeuchi, M.; Nakayama, M.; Shiiba, H.; Ogawa, M.; Nakayama, K.; Ohta, T.; Endo, D.; Ozaki, T.; Inamasu, T.; Sato, K.; Komaba, S. High-capacity electrode materials for rechargeable lithium batteries: Li_3NbO_4 -based system with cation-disordered rocksalt structure. *Proc. Natl. Acad. Sci. U.S.A.* **2015**, *112*, 7650–7655.
- (11) Wang, R.; Li, X.; Liu, L.; Lee, J.; Seo, D.-H.; Bo, S.-H.; Urban, A.; Ceder, G. A disordered rock-salt Li-excess cathode material with high capacity and substantial oxygen redox activity: $\text{Li}_{1.25}\text{Nb}_{0.25}\text{Mn}_{0.5}\text{O}_2$. *Electrochem. Commun.* **2015**, *60*, 70–73.
- (12) House, R. A.; Jin, L.; Maitra, U.; Tsuruta, K.; Somerville, J. W.; Förstermann, D. P.; Massel, F.; Duda, L.; Roberts, M. R.; Bruce, P. G. Lithium manganese oxyfluoride as a new cathode material exhibiting oxygen redox. *Energy Environ. Sci.* **2018**, *11*, 926–932.
- (13) Lee, J.; Seo, D.-H.; Balasubramanian, M.; Twu, N.; Li, X.; Ceder, G. A new class of high capacity cation-disordered oxides for rechargeable lithium batteries: Li–Ni–Ti–Mo oxides. *Energy Environ. Sci.* **2015**, *8*, 3255–3265.
- (14) Zhao, E.; Li, Q.; Meng, F.; Liu, J.; Wang, J.; He, L.; Jiang, Z.; Zhang, Q.; Yu, X.; Gu, L.; Yang, W.; Li, H.; Wang, F.; Huang, X. Stabilizing the Oxygen Lattice and Reversible Oxygen Redox Chemistry through Structural Dimensionality in Lithium-Rich Cathode Oxides. *Angew. Chem., Int. Ed.* **2019**, *58*, 4323–4327.
- (15) Zhao, E.; He, L.; Wang, B.; Li, X.; Zhang, J.; Wu, Y.; Chen, J.; Zhang, S.; Liang, T.; Chen, Y.; Yu, X.; Li, H.; Chen, L.; Huang, X.; Chen, H.; Wang, F. Structural and mechanistic revelations on high capacity cation-disordered Li-rich oxides for rechargeable Li-ion batteries. *Energy Storage Mater.* **2019**, *16*, 354–363.
- (16) Ji, H.; Kitchaev, D. A.; Lun, Z.; Kim, H.; Foley, E.; Kwon, D.-H.; Tian, Y.; Balasubramanian, M.; Bianchini, M.; Cai, Z.; Clément, R. J.; Kim, J. C.; Ceder, G. Computational investigation and experimental realization of disordered high-capacity Li-ion cathodes based on Ni redox. *Chem. Mater.* **2019**, *31*, 2431–2442.
- (17) Chen, R.; Ren, S.; Knapp, M.; Wang, D.; Witter, R.; Fichtner, M.; Hahn, H. Disordered lithium-rich oxyfluoride as a stable host for enhanced Li^+ intercalation storage. *Adv. Energy Mater.* **2015**, *5*, No. 1401814.
- (18) Chen, R.; Ren, S.; Yavuz, M.; Guda, A. A.; Shapovalov, V.; Witter, R.; Fichtner, M.; Hahn, H. Li^+ intercalation in isostructural Li_2VO_3 and $\text{Li}_2\text{VO}_2\text{F}$ with O^{2-} and mixed O^{2-}/F^- anions. *Phys. Chem. Chem. Phys.* **2015**, *17*, 17288–17295.
- (19) Källquist, I.; Naylor, A. J.; Baur, C.; Chable, J.; Kullgren, J.; Fichtner, M.; Edström, K.; Brandell, D.; Hahlin, M. Degradation mechanisms in $\text{Li}_2\text{VO}_2\text{F}$ Li-rich disordered rock-salt cathodes. *Chem. Mater.* **2019**, *31*, 6084–6096.
- (20) Baur, C.; Källquist, I.; Chable, J.; Chang, J. H.; Johnsen, R. E.; Ruiz-Zepeda, F.; Ateba Mba, J.-M.; Naylor, A. J.; Garcia-Lastra, J. M.; Vegge, T.; Klein, F.; Schür, A. R.; Norby, P.; Edström, K.; Hahlin, M.; Fichtner, M. Improved cycling stability in high-capacity Li-rich vanadium containing disordered rock salt oxyfluoride cathodes. *J. Mater. Chem. A* **2019**, *7*, 21244–21253.
- (21) Liu, S.; Feng, X.; Wang, X.; Shen, X.; Hu, E.; Xiao, R.; Yu, R.; Yang, H.; Song, N.; Wang, Z.; Yang, X.; Chen, L. Another strategy, detouring potential decay by fast completion of cation mixing. *Adv. Energy Mater.* **2018**, *8*, No. 1703092.
- (22) Hoshino, S.; Glushenkov, A. M.; Ichikawa, S.; Ozaki, T.; Inamasu, T.; Yabuuchi, N. Reversible three-electron redox reaction of $\text{Mo}^{3+}/\text{Mo}^{6+}$ for rechargeable lithium batteries. *ACS Energy Lett.* **2017**, *2*, 733–738.
- (23) Yabuuchi, N.; Nakayama, M.; Takeuchi, M.; Komaba, S.; Hashimoto, Y.; Mukai, T.; Shiiba, H.; Sato, K.; Kobayashi, Y.; Nakao, A.; Yonemura, M.; Yamanaka, K.; Mitsuhara, K.; Ohta, T. Origin of stabilization and destabilization in solid-state redox reaction of oxide ions for lithium-ion batteries. *Nat. Commun.* **2016**, *7*, No. 13814.
- (24) Chen, D.; Wu, J.; Papp, J. K.; McCloskey, B. D.; Yang, W.; Chen, G. Role of redox-inactive transition-metals in the behavior of cation-disordered rocksalt cathodes. *Small* **2020**, *16*, No. e2000656.
- (25) Lee, J.; Papp, J. K.; Clement, R. J.; Sallis, S.; Kwon, D. H.; Shi, T.; Yang, W.; McCloskey, B. D.; Ceder, G. Mitigating oxygen loss to improve the cycling performance of high capacity cation-disordered cathode materials. *Nat. Commun.* **2017**, *8*, No. 981.
- (26) Sato, T.; Sato, K.; Zhao, W.; Kajiyama, Y.; Yabuuchi, N. Metastable and nanosize cation-disordered rocksalt-type oxides: revisit of stoichiometric LiMnO_2 and NaMnO_2 . *J. Mater. Chem. A* **2018**, *6*, 13943–13951.
- (27) Qi, R.; CampÉon, B. D. L.; Konuma, I.; Sato, Y.; Kaneda, Y.; Kondo, M.; Yabuuchi, N. Metastable and nanosized $\text{Li}_{1.2}\text{Nb}_{0.2}\text{V}_{0.6}\text{O}_2$ for high-energy Li-ion batteries. *Electrochemistry* **2022**, *90*, No. 037005.
- (28) Cai, Z.; Zhang, Y. Q.; Lun, Z.; Ouyang, B.; Gallington, L. C.; Sun, Y.; Hau, H. M.; Chen, Y.; Scott, M. C.; Ceder, G. Thermodynamically driven synthetic optimization for cation-disordered rock salt cathodes. *Adv. Energy Mater.* **2022**, *12*, No. 2103923.
- (29) Ouyang, B.; Artrith, N.; Lun, Z.; Jadidi, Z.; Kitchaev, D. A.; Ji, H.; Urban, A.; Ceder, G. Effect of fluorination on lithium transport and short-range order in disordered-rocksalt-type lithium-ion battery cathodes. *Adv. Energy Mater.* **2020**, *10*, No. 1903240.
- (30) Ji, H.; Urban, A.; Kitchaev, D. A.; Kwon, D. H.; Artrith, N.; Ophus, C.; Huang, W.; Cai, Z.; Shi, T.; Kim, J. C.; Kim, H.; Ceder, G. Hidden structural and chemical order controls lithium transport in

cation-disordered oxides for rechargeable batteries. *Nat. Commun.* **2019**, *10*, No. 592.

(31) Clément, R. J.; Kitchaev, D.; Lee, J.; Gerbrand, C. Short-range order and unusual modes of nickel redox in a fluorine-substituted disordered rocksalt oxide lithium-ion cathode. *Chem. Mater.* **2018**, *30*, 6945–6956.

(32) Kan, W. H.; Deng, B.; Xu, Y.; Shukla, A. K.; Bo, T.; Zhang, S.; Liu, J.; Pianetta, P.; Wang, B.-T.; Liu, Y.; Chen, G. Understanding the effect of local short-range ordering on lithium diffusion in $\text{Li}_{1.3}\text{Nb}_{0.3}\text{Mn}_{0.4}\text{O}_2$ single-crystal cathode. *Chem* **2018**, *4*, 2108–2123.

(33) Jones, M. A.; Reeves, P. J.; Seymour, I. D.; Cliffe, M. J.; Dutton, S. E.; Grey, C. P. Short-range ordering in a battery electrode, the 'cation-disordered' rocksalt $\text{Li}_{1.25}\text{Nb}_{0.25}\text{Mn}_{0.5}\text{O}_2$. *Chem. Commun.* **2019**, *55*, 9027–9030.

(34) Lun, Z.; Ouyang, B.; Kwon, D. H.; Ha, Y.; Foley, E. E.; Huang, T. Y.; Cai, Z.; Kim, H.; Balasubramanian, M.; Sun, Y.; Huang, J.; Tian, Y.; Kim, H.; McCloskey, B. D.; Yang, W.; Clement, R. J.; Ji, H.; Ceder, G. Cation-disordered rocksalt-type high-entropy cathodes for Li-ion batteries. *Nat. Mater.* **2021**, *20*, 214–221.

(35) Diaz-Lopez, M.; Chater, P. A.; Proux, O.; Joly, Y.; Hazemann, J.-L.; Bordet, P.; Pralong, V. Li trapping in nanolayers of cation 'disordered' rock salt cathodes. *J. Mater. Chem. A* **2022**, *10*, 17415–17423.

(36) Wang, Y.; Huang, S.; Raji-Adefila, B.; Outka, A.; Wang, J. H.; Chen, D. Unraveling the nature and role of layered cation ordering in cation-disordered rock-salt cathodes. *J. Am. Chem. Soc.* **2022**, *144*, 19838–19848.

(37) Urban, A.; Abdellahi, A.; Dacek, S.; Artrith, N.; Ceder, G. Electronic-structure origin of cation disorder in transition-metal oxides. *Phys. Rev. Lett.* **2017**, *119*, No. 176402.

(38) Kan, W. H.; Wei, C.; Chen, D.; Bo, T.; Wang, B. T.; Zhang, Y.; Tian, Y.; Lee, J. S.; Liu, Y.; Chen, G. Evolution of local structural ordering and chemical distribution upon delithiation of a rock salt-structured $\text{Li}_{1.3}\text{Ta}_{0.3}\text{Mn}_{0.4}\text{O}_2$ cathode. *Adv. Funct. Mater.* **2019**, *29*, No. 1808294.

(39) Huang, J.; Zhong, P.; Ha, Y.; Kwon, D.-H.; Crafton, M. J.; Tian, Y.; Balasubramanian, M.; McCloskey, B. D.; Yang, W.; Ceder, G. Non-topotactic reactions enable high rate capability in Li-rich cathode materials. *Nat. Energy* **2021**, *6*, 706–714.

(40) Kwon, D.-H.; Lee, J.; Artrith, N.; Kim, H.; Wu, L.; Lun, Z.; Tian, Y.; Zhu, Y.; Ceder, G. The impact of surface structure transformations on the performance of Li-excess cation-disordered rocksalt cathodes. *Cell Rep. Phys. Sci.* **2020**, *1*, No. 100187.

(41) McGreevy, R. L.; Pusztai, L. Reverse Monte Carlo simulation: A new technique for the determination of disordered structures. *Mol. Simul.* **1988**, *1*, 359–367.

(42) McGreevy, R. L. Reverse monte carlo modelling. *J. Phys.: Condens. Matter* **2001**, *13*, R877–R913.

(43) Keen, D. A.; McGreevy, R. L. Structural modelling of glasses using reverse Monte Carlo simulation. *Nature* **1990**, *344*, 423–425.

(44) Thomson, K. T.; Gubbins, K. E. Modeling structural morphology of microporous carbons by reverse monte carlo. *Langmuir* **2000**, *16*, 5761–5773.

(45) Pikunic, J.; Clinard, C.; Cohaut, N.; Gubbins, K. E.; Guet, J.-M.; Pellenq, R. J. M.; Rannou, I.; Rouzaud, J.-N. Structural modeling of porous carbons: Constrained reverse monte carlo method. *Langmuir* **2003**, *19*, 8565–8582.

(46) Jain, S. K.; Pellenq, R. J.; Pikunic, J. P.; Gubbins, K. E. Molecular modeling of porous carbons using the hybrid reverse Monte Carlo method. *Langmuir* **2006**, *22*, 9942–9948.

(47) Keen, D. A.; Tucker, M. G.; Dove, M. T. Reverse monte carlo modelling of crystalline disorder. *J. Phys.: Condens. Matter* **2005**, *17*, S15–S22.

(48) Jiang, B.; Bridges, C. A.; Unocic, R. R.; Pitike, K. C.; Cooper, V. R.; Zhang, Y.; Lin, D. Y.; Page, K. Probing the local site disorder and distortion in pyrochlore high-entropy oxides. *J. Am. Chem. Soc.* **2021**, *143*, 4193–4204.

(49) Kitamura, N.; Tanabe, Y.; Ishida, N.; Idemoto, Y. The atomic structure of a MgCo_2O_4 nanoparticle for a positive electrode of a Mg rechargeable battery. *Chem. Commun.* **2019**, *55*, 2517–2520.

(50) Kitamura, N.; Kubo, Y.; Ishida, N.; Idemoto, Y. Study of atomic ordering across the layer in lithium-rich layered positive electrode material towards preparation process optimization. *J. Power Sources* **2019**, *437*, No. 226905.

(51) Huang, Y.; Liu, L.; Zhu, Y.; Gao, M.; Zhang, J. A new model on cation distribution in cation-disordered $\text{Li}_{1+x}\text{TM}_{1-x}\text{O}_2$ cathodes. *Solid State Ionics* **2020**, *351*, No. 115341.

(52) Semykina, D. O.; Morkhova, Y. A.; Kabanov, A. A.; Mishchenko, K. V.; Slobodyuk, A. B.; Kirsanova, M. A.; Podgornova, O. A.; Shindrov, A. A.; Okhotnikov, K. S.; Kosova, N. V. Effect of transition metal cations on the local structure and lithium transport in disordered rock-salt oxides. *Phys. Chem. Chem. Phys.* **2022**, *24*, 5823–5832.

(53) Ok, K. M.; Halasyamani, P. S.; Casanova, D.; Llundell, M.; Alemany, P.; Alvarez, S. Distortions in octahedrally coordinated d0 transition metal oxides: A continuous symmetry measures approach. *Chem. Mater.* **2006**, *18*, 3176–3183.

(54) Zhou, K.; Zheng, S.; Liu, H.; Zhang, C.; Gao, H.; Luo, M.; Xu, N.; Xiang, Y.; Liu, X.; Zhong, G.; Yang, Y. Elucidating and mitigating the degradation of cationic-anionic redox processes in $\text{Li}_{1.2}\text{Mn}_{0.4}\text{Ti}_{0.4}\text{O}_2$ cation-disordered cathode materials. *ACS Appl. Mater. Interfaces* **2019**, *11*, 45674–45682.

(55) Zheng, S.; Zhou, K.; Zheng, F.; Liu, H.; Zhong, G.; Zuo, W.; Xu, N.; Zhao, G.; Luo, M.; Wu, J.; Zhang, C.; Zhang, Z.; Wu, S.; Yang, Y. Mn^{4+} -substituted Li-Rich $\text{Li}_{1.2}\text{Mn}_{0.4}^{3+}\text{Mn}_x^{4+}\text{Ti}_{0.4-x}^{4+}\text{O}_2$ materials with high energy density. *ACS Appl. Mater. Interfaces* **2020**, *12*, 40347–40354.